M.A. Zocher, T.D. Aslam, S.I. Jackson, and E.K. Anderson.
"Numerical Modeling Comparing Slab to Cylinder Test Expansion Geometries for PBX 9501."
In Proceedings of the 16th International Detonation Symposium (Office of Naval Research, 2019).

Numerical Modeling Comparing Slab to Cylinder Test Expansion Geometries for PBX 9501

Marvin A. Zocher, Tariq D. Aslam, Scott I. Jackson, and Eric K. Anderson

Los Alamos National Laboratory, Los Alamos, NM, USA 87545

Abstract. Numerical modeling of experiments conducted using two distinct types of high explosive (HE) expansion test geometries (slab and cylinder) is conducted. Viability of the slab expansion test as an alternative to the cylinder expansion test for an assessment of HE behavior and model validation is demonstrated. Simulations using a proposed set of phenomenological parameters for the constitutive and detonation behavior of PBX 9501 is found to provide reasonably good agreement between simulation and empirical data.

Introduction

For many years now the high explosive cylinder expansion test has been a tool often used for the purpose of investigating detonation and the constitutive response of HE reactants and products, and for validating numerical models thereof. The test normally involves the initiation of detonation at one end of a cylinder of HE that is encased circumferentially in a thin metallic cylindrical sleeve (the metallic sleeve is open-ended). As the detonation wave propagates through the length of the cylinder, the metallic confinement expands. By carefully measuring this expansion, one may gain valuable insight into detonation propagation as well as the constitutive behavior of reactants and products, and can use the measurements of cylinder expansion for quantitative model validation, comparing predicted expansion to that which is measured.

A planar analog to the cylinder expansion test that has recently been developed [1] can be referred to as a slab expansion test [2]. In this test a planar slab of HE is sandwiched between two thin layers of metal. Detonation in the HE is initiated by a line wave generator (LWG). As the detonation sweeps through the length of the slab, the sandwiching metallic layers deflect outward. As with the cylinder test, careful measurement of the movement of metal can be used to gain valuable insight into detonation and constitutive behavior, and to evaluate models, comparing predicted to measured motion. In both cases (cylinder and slab) the primary empirical diagnostic is Photon Doppler Velocimetry (PDV) measurement of free-surface velocity.

Our objectives in this work are two-fold: (1) to demonstrate the viability of using the slab expansion test as an alternative to the well-known cylinder expansion test for HE behavior observation and for model validation, and (2) to evaluate a proposed set of phenomenological parameters for modeling the constitutive (two-part Davis-type equation of state (EOS)) and detonation (Wescott-Stewart-Davis reactive burn model) behavior of PBX 9501. In partial fulfillment of this objective we conduct numerical modeling of two experiments that were recently conducted at Los Alamos National Laboratory, one of each experimental type (slab and cylinder). Numerical prediction is compared to empirical data.

The numerical analysis is conducted using the Los Alamos finite volume continuum mechanics code FLAG[3].

The Experiments

Since the focus of this work is modeling, as opposed to experimental methodologies, only a cursory discussion pertaining to details of the experiments will be provided here. The interested reader is referred to Jackson *et al.* [2] for a discussion of experimental detail.

HE Cylinder Expansion Test

The HE cylinder test specimen used in this study (Test No. 8-1964) was assembled using twelve pellets of PBX 9501 (2.54 cm in length and 2.54 cm in diameter) encased in an annealed Cu sleeve. The pellets were carefully placed so as to minimize any trapped air. For purposes of numerical modeling (discussed later) the diameter of the HE was assumed to be 2.5446 cm and the thickness of the copper sleeve 0.2523 cm. Detonation in the PBX 9501 was initiated by an RP-1 detonator. A drawing of the as-modeled cylinder test specimen is provided in Figure 1.

Diagnostics included PDV with measurements of free-surface velocity taken at 8 locations: Z_P (see Fig. 1) = 20.0025, 20.3200, 20.3200, 20.3200, 22.8600, 22.8600, 22.7025, and 22.8600 cm for Probes 1-8, respectively. We need not address azimuth since this detail is irrelevant with respect to the present work. All eight PDV probes were aligned normal to the Cu sleeve. Shorting wires were used for a measurement of detonation speed. A streak camera was used to capture an image of the breakout surface along a center chord.

HE Slab Expansion Test

The HE slab test (Test No. 8-1932) was conducted using PBX 9501 bonded to Cu plates. For purposes of numerical modeling (discussed later) the thickness of the HE was assumed to be 1.003 cm, and the thickness of the copper plates to be 0.102 cm. Detonation in the PBX 9501 was initiated by a LWG. A drawing of the as-modeled slab test specimen is provided in Figure 2.

Diagnostics included PDV with measurements of free-surface velocity taken at 4 locations (see Fig. 2). All PDV probes were aligned normal to the Cu plates. In addition to PDV, shorting wires were used to measure detonation speed.

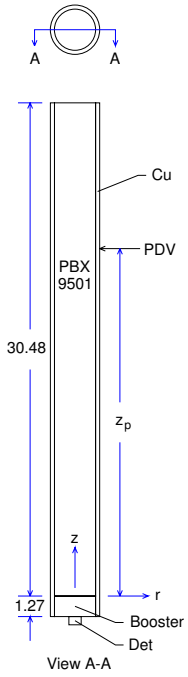

Fig. 1: Cylindrical geometry. All dimensions in cm.

HE Constitutive and Reactive Burn Models

HE detonation and constitutive behavior are modeled in this work using the WSD reactive burn model in concert with a two-part EOS for the PBX 9501. We have chosen to use Davis-type [4] EOSs for both reactants and products.

Davis-type EOS for Reactants

Reference [4] gives equations for $p = p(v, E)$ and $T = T(v, E)$ where p, T, v, and E denote pressure, temperature, specific volume, and specific internal energy, respectively. We can equivalently express equations for p and T in terms of density, ρ, and specific internal energy (here we will use e instead of E to denote specific internal energy), that is, $p = p(\rho, e)$ and $T = T(\rho, e)$. Doing so yields:

$$p(\rho, e) = p_s(\rho) + \rho\,\Gamma(\rho)\,[e - e_s(\rho)] \tag{1}$$

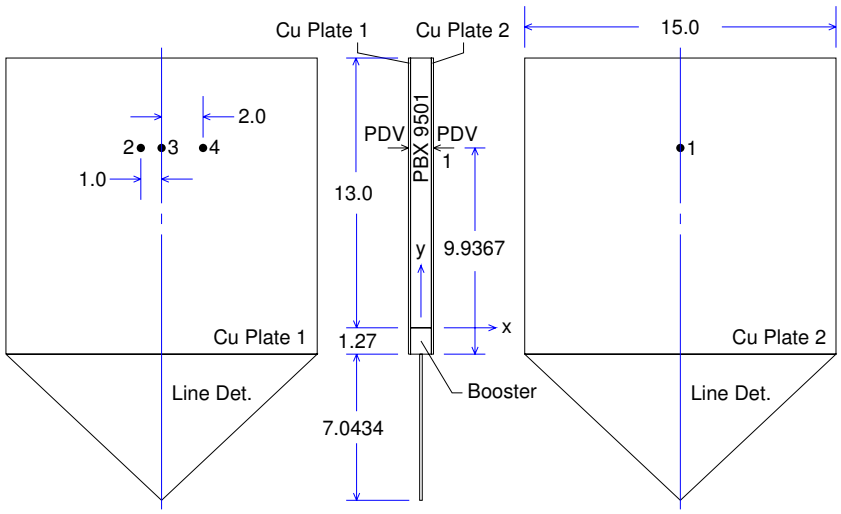

Fig. 2: Slab geometry. Bold numbers 1, 2, 3, 4 denote probe IDs. Black dots denote PDV illumination points. All dimensions in cm.

$$T(\rho, e) = T_s(\rho)\Psi_1^{\frac{1}{1+\alpha_{st}}} \tag{2}$$

where,

$$\Psi_1 = \left\{ \frac{1+\alpha_{st}}{C_{v0}T_s(\rho)} \left[(e - e_s(\rho)\right] + 1 \right\} \tag{3}$$

$$p_s(\rho) = \begin{cases} \hat{p}\left[\sum_{j=1}^{3} \Psi_2 + \Psi_3\right] & \rho \geq \rho_0 \\ \\ \hat{p}\left[\exp\left(4By\right) - 1\right] & \rho < \rho_0 \end{cases} \tag{4}$$

$$\Psi_2 = \frac{(4By)^j}{j!};\ \Psi_3 = \frac{C\,(4By)^4}{4!} + \frac{y^2}{(1-y)^4} \tag{5}$$

$$e_s(\rho) = \frac{1}{\rho_0}\int_0^y p_s(\xi)\, d\xi \tag{6}$$

$$\Gamma(\rho) = \begin{cases} \Gamma_0 + Zy & \rho \geq \rho_0 \\ \\ \Gamma_0 & \rho < \rho_0 \end{cases} \tag{7}$$

$$\hat{p} = \frac{\rho_0 A^2}{4B} \tag{8}$$

$$y = 1 - \frac{\rho_0}{\rho} \tag{9}$$

$$T_s(\rho) = \begin{cases} T_0 \left(\frac{\rho}{\rho_0}\right)^{\Gamma_0} & \rho < \rho_0 \\ \\ T_0\, e^{-Zy} \left(\frac{\rho}{\rho_0}\right)^{(\Gamma_0 + Z)} & \rho \geq \rho_0 \end{cases} \tag{10}$$

In Equations 1-10, e_s, p_s, and T_s are the specific internal energy, pressure, and temperature on the isentrope passing through reference density, ρ_0, respectively, Γ is the Grüneisen gamma, and A, B, C, α_{st}, C_{v0}, Γ_0, v_0, T_0, and Z are model parameters. Note that the term E_0 appearing in Equation (26) of Ref. [4] is omitted from our Equation 6 (the term corresponding to E_0 (e_0 in our notation) is handled elsewhere in FLAG).

Davis-type EOS for Products

As was the case for the reactants EOSs, the Davis-type EOSs for products as delineated in

Ref. [4] are given in in terms of specific volume and specific energy, that is, $p = p(v, E)$ and $T = T(v, E)$. Also as was done for reactants, we shall equivalently express equations for p and T in terms of density and specific internal energy (and as in the previous section we shall use e to denote specific internal energy as opposed to E, which was used in Ref. [4]).

$$p(\rho, e) = p_s(\rho) + \rho\,\Gamma(\rho)\,[e - e_s(\rho)] \tag{11}$$

$$T(\rho, e) = T_s(\rho) + \frac{e - e_s(\rho)}{C_v} \tag{12}$$

where,

$$p_s(\rho) = p_c\,\frac{\Psi_4^{a/n}}{\left(\frac{1}{\rho v_c}\right)^{k+a}}\,\frac{(k-1+F(\rho))}{(k-1+a)} \tag{13}$$

$$\Psi_4 = \left[\frac{1}{2}\left(\frac{1}{\rho v_c}\right)^{n} + \frac{1}{2}\left(\frac{1}{\rho v_c}\right)^{-n}\right] \tag{14}$$

$$e_s(\rho) = e_c\,\frac{\Psi_4^{a/n}}{\left(\frac{1}{\rho v_c}\right)^{k-1+a}} - e_0 \tag{15}$$

$$\Gamma(\rho) = k - 1 + (1-b)F(\rho) \tag{16}$$

$$F(\rho) = \frac{2a\left(\frac{1}{\rho v_c}\right)^{-n}}{\left(\frac{1}{\rho v_c}\right)^{n} + \left(\frac{1}{\rho v_c}\right)^{-n}} \tag{17}$$

$$e_c = \frac{p_c v_c}{k-1+a} \tag{18}$$

$$T_s(\rho) = T_c\,\frac{\Psi_4^{(a/n)(1-b)}}{\left(\frac{1}{\rho v_c}\right)^{k-1+a(1-b)}} \tag{19}$$

$$T_c = \left[\frac{2^{-ab/n}}{k-1+a}\right]\frac{p_c v_c}{C_v} \tag{20}$$

In Equations 11-20 a, b, k, n, p_c, v_c, C_v, and e_0 are model parameters. Note that the term e_0 appearing in Equation 15 does not appear in Equation (6) of Ref. [4].

WSD Reactive Burn Model

The reactive burn model as delineated in Ref. [4] can be expressed in a generalized yet precisely equivalent form as:

$$R = R_I + R_{IG} + R_{DG} + R_B \tag{21}$$

where

$$R_I = r_i\,\Psi_5\,(1-\lambda)^{r_b}\,\Psi_6\,\Psi_7 \tag{22}$$

$$\Psi_5 = \left(\frac{\rho}{\rho_0} - 1 - r_a\right)^{r_x} \tag{23}$$

$$\Psi_6 = H\left(\frac{\rho}{\rho_0} - 1 - r_a\right) \tag{24}$$

$$\Psi_7 = \frac{1}{2}\left[1 - \tanh\left\{200(\lambda - 0.025)\right\}\right] \tag{25}$$

$$R_{IG} = r_{g1}\,(1-\lambda)^{r_c}\,\lambda^{r_d} p^{r_y}\,\Psi_8\Psi_9 \tag{26}$$

$$\Psi_8 = \frac{1}{2}\left[1 - \tanh\left\{30\,(\lambda - r_{\text{switch}})\right\}\right] \tag{27}$$

$$\Psi_9 = \frac{1}{2}\left[1 - \tanh\left\{50\left(\frac{\rho_{SH}}{\rho_c} - 1\right)\right\}\right] \tag{28}$$

$$R_{DG} = r_k\,(1-\lambda)^{r_c}\,\lambda^{r_d} p^{r_n}\,\Psi_8\,\Psi_{10} \tag{29}$$

$$\Psi_{10} = \frac{1}{2}\left[1 + \tanh\left\{50\left(\frac{\rho_{SH}}{\rho_c} - 1\right)\right\}\right] \tag{30}$$

$$R_{_B} = r_{_{g2}}\,(1-\lambda)^{r_e}\,p^{r_z}\,\Psi_{11} \tag{31}$$

$$\Psi_{11} = \frac{1}{2}\left[1 + \tanh\left\{30\left(\lambda - r_{\rm switch}\right)\right\}\right] \tag{32}$$

Equations 21-32 are what is programmed into FLAG. In these equations, r_a, r_b, r_c, r_d, r_e, r_i, r_k, r_n, r_x, r_y, r_z, r_{g1}, r_{g2}, ρ_0, ρ_c, and $r_{\rm switch}$ are model parameters. Additional model parameters that do not appear in eqs. 21- 32 include: rkdead (rate constant in preshock desensitization), rpign (minimum pressure to start burn), rpmax (maximum pressure at which to deaden), and rphel (Hugoniot elastic limit minimum to desensitize). These last four parameters are included for completeness, though they are not used in our analysis since rkdead is set to zero. These parameters are discussed in Wescott *et al.* [5]

It is worth noting that for the parameter set used in this work (provided in the next section), the WSD burn model simplifies drastically from that shown in equations 21-32. In fact, since (as will be seen in the next section), r_i and r_d are set to 0, r_b = r_c = r_e, r_n = r_y = r_z, and r_{g1} = r_{g2} = r_k, the reaction rate becomes (as given in Ref. [6]):

$$R = a\,(1-\lambda)^{\nu}\left(\frac{p}{B}\right)^{N_p} \tag{33}$$

where a, ν, B, and N_p are model parameters.

It is also worth noting that the reaction rate equation, Eq. 33, can be generalized to include an Arrhenius term (commonly included when dealing with gaseous detonation). This was done, *e.g*, in [7] where the rate equation is expressed as:

$$R = a\,(1-\lambda)^{\nu}\left(\frac{p}{B}\right)^{N_p}\exp\left(\frac{-\rho E}{p}\right) \tag{34}$$

where E is the activation energy.

For our purposes, it is the equation set 21-32 that is most pertinent since this more general form represents what is programmed into FLAG.

Parameter Sets

The parameter sets used in this work are provided in Tables 1-3.

Table 1: Davis reactants parameter set

Parameter	Value
A	0.21 $(\mathrm{cm})(\mu\mathrm{s})^{-1}$
B	3.8
C	0.4
α_{st}	0.3662
C_{v0}	10.67x10^{-6} $(\mathrm{Mbar\ cm^3})(\mathrm{gK})^{-1}$
Γ_0	0.67
ρ_0	1.832 $(\mathrm{g})(\mathrm{cm^3})^{-1}$
T_0	297 K
Z	0.0

Table 2: Davis products parameter set

Parameter	Value
a	0.867302
b	1.04
C_v	4.34x10^{-6} $(\mathrm{Mbar\ cm^3})(\mathrm{gK})^{-1}$
e_0	0.0566997 $(\mathrm{Mbar\ cm^3})(\mathrm{g})^{-1}$
k	1.33
n	1.00164
p_c	0.0282 Mbar
v_c	0.95 $(\mathrm{cm^3})(\mathrm{g})^{-1}$

Numerical Modeling

As mentioned already, all numerical analysis conducted in this work was accomplished using the FLAG finite volume continuum mechanics code (Version 3.8.Alpha.2). FLAG is an ALE code that can be used to approximate the solution to initial boundary value problems and can be executed in 1d, 2d, or 3d geometric complexity. It has slideline and slide surface capabilities. It incorporates a number of mesh relaxation schemes.

Simplifications and Approximations

The reader who compares the experimental assemblies depicted in Figs. 1-2 to those described in Ref. [2] will note that a number of simplifications have been taken in our modeling. For example, in both cases (cylinder and slab), we have ignored complicating features that are not expected to significantly impact the accuracy of our modeling, such as base plates, mounting brackets, glue and the like. The astute reader may also note that Figs. 1-2 show the presence of boosters that do not exist in the experiment. In both cases (cylinder and

Table 3: WSD parameter set

Parameter	Value
r_a	0.214
r_b	0.9562
r_c	0.9562
r_d	0.0
r_e	0.9562
r_{g1}	6377.78 $\left(\mu\mathrm{s}\,\mathrm{Mbar}^{3.3898}\right)^{-1}$
r_{g2}	6377.78 $\left(\mu\mathrm{s}\,\mathrm{Mbar}^{3.3898}\right)^{-1}$
r_i	0.0 $\mu\mathrm{s}^{-1}$
r_k	6377.78 $\left(\mu\mathrm{s}\,\mathrm{Mbar}^{3.3898}\right)^{-1}$
r_n	3.3898
r_x	7.0
r_y	3.3898
r_z	3.3898
ρ_0	1.844 $(\mathrm{g})(\mathrm{cm}^3)^{-1}$
ρ_c	2.740 $(\mathrm{g})(\mathrm{cm}^3)^{-1}$
r_{switch}	0.90
rkdead	0.0 $\mu\mathrm{s}^{-1}$
rpign	1x10^{-5} Mbar
rpmax	0.06 Mbar
rphel	0.0007 Mbar

slab) the detonator (either RP-1 or LWG) were actually in intimate contact with the PBX 9501 (at $z = 0$ in the one case, and $y = 0$ in the other). Rather than modeling the detonation initiation devices (either RP-1 or LWG) directly, we chose to "mimic" their impact through the use of a booster. The booster was modeled as a hybrid material with the constitutive response of PBX 9407 (two-part Grüneisen/JWL EOS) and with detonation propagation accomplished *via* detonation shock dynamics (DSD) [8] using DSD parameters derived for PBX 9501. Taking this approach resulted in smooth initiation of the PBX 9501 at location $z = 0$ (cylinder) or at location $y = 0$ (slab) at a time slightly later than $t = 0$. Thus what was modeled with respect to detonation initiation is not precisely what occured in the experiments, but the approximations made are far enough removed from the location of diagnostics that they are not expected to have a profound impact upon our analysis.

Modeling the HE Cylinder Expansion Experiment

The HE cylinder expansion experiment (8-1964) was modeled in FLAG as a 2d axially-symmetric initial boundary value problem. Mesh discretization resulted in an average element size of 100 μm. Boundary conditions were set such that nodes at top and bottom of the assemblage could move in the r-direction but not in the z-direction. PBX 9501 constitutive response was modeled using a two-part Davis EOS as described in the previous section. Detonation within the PBX 9501 was modeled using WSD reactive burn as described in the previous section. Deviatoric constitutive behavior of the copper was modeled using the PTW [9] flow stress model. No slide lines were employed. Nodal relaxation was employed using the feasibility set method [10] and a strobing controller such that relaxation was on for 1 cycle, off for 60 cycles, repeating, starting from 1.00 μs.

Modeling the HE Slab Expansion Experiment

The HE slab expansion experiment (8-1932) was modeled in FLAG as a 2d cartesian initial boundary value problem. Average cell size was 100 μm. Boundary conditions were set such that nodes at top and bottom of the assemblage could move in the x-direction but not in the y-direction. Note that since the modeling was done in 2d, only the data from Probes 1 and 3 are relevant to the analysis; to make use of the data from Probes 2 and 4 we must run the simulation in 3d. The high explosives and Cu were modeled as described in the previous section. No slide lines were employed. Nodal relaxation was employed as described in the previous sub-section.

Modeling Results

Simulation results for the cylinder expansion test are provided in Figs. 3-6 and 11. Cross-sectional images of the cylindrical assemblage are shown in Fig. 3. Pressure profiles are shown in Fig. 4. In Fig. 5 we "zoom in" on various portions of the images shown in Fig. 4 to try to highlight features where the pressure gradient is highest. Figure 6 privides the color palette for Figs 4 and 5. Figure 11 provides: LHS: a comparison of predicted free surface velocity to empirical data for a representative probe (comparisons to the data from other probes

look similar), and RHS: pressure history for an arbitrary but representative point. Figures. 7-10 and 12 are analagous to Figs. 3-6 and 11, but are for the slab expansion test. All results shown derive from Simulations R029 for the cylinder test, and R004 for the slab test.

It should be noted that using a 100 μm mesh results in an over-prediction of detonation velocity. Our calculated value of detonation velocity is approximately 9.0 km/s, whereas the experimentally-determined value is closer to 8.8 km/s. The suspected reason for this discrepancy is that the reaction zone for PBX 9501 is on the order of 10 μm and that to get the calculated determination of detonation velocity right, we need to model with a mesh resolution of similar order. We have not yet successfully modeled with such a fine mesh resolution. Note that since $t = 0$ is somewhat arbitrary in the experiment, jump-off times are aligned in Figs. 11 and 12, as is rather customary.

Conclusions

Despite some rather gross simplifications that were employed (*e.g.*, ignoring mounting plates, brackets, and the like), our predictions of free-surface velocity match the measured velocities rather well. This is true whether we compare to the cylinder expansion test or the slab expansion test. This observation supports the assertion that the slab expansion test is indeed a viable alternative to the well-known cylinder expansion test for HE behavior observations and for model validation purposes. Relatively good agreement between simulation and empirical data also gives us some confidence with respect to the parameterization of our constitutive and detonation models, though some refinement in this regard may ultimately prove to be warranted. Refinement will likely, for example, improve our under-prediction of velocity in the first few ring-ups and over-prediction of velocity at mid-range or late time (see Figs. 11 and 12).

References

1. Hill, L., "Development of the LANL Sandwich Test," in "Shock Compression of Condensed Matter – 2001," , edited by Furnish, M., Thadhani, N. and Horie, Y., pp. 149–152, AIP Proceedings No. 620, 2003.

2. Jackson, S., Anderson, E., Aslam, T., Whitley, V. and Zocher, M., "Comparison of Slab and Cylinder Test Expansion Geometries for PBX 9501," Technical Report LA-UR 17-25358, Los Alamos National Laboratory, Los Alamos, NM, USA, 2017.

3. Burton, D., "Lagrangian Hydrodynamics in the FLAG code," Technical Report LA-UR 07-7545, Los Alamos National Laboratory, Los Alamos, NM, USA, 2007.

4. Wescott, B., Stewart, D. and Davis, W., "Equation of State and Reaction Rate for Condensed-Phase Explosives," *Journal of Applied Physics*, Vol. 98, pp. 053514(1–10), 2005.

5. Wescott, B., Stewart, D. and Davis, W., "Modeling Detonation Diffraction and Dead Zones in PBX-9502," in "Proc., 13th International Detonation Symposium," pp. 744–750, Office of Naval Research, ONR 351-07-01, 2006.

6. Lambert, D., Stewart, D., Yoo, S. and Wescott, B., "Experimental Validation of Detonation Shock Dynamics in Condensed Explosives," *Journal of Fluid Mechanics*, Vol. 546, pp. 227–253, 2006.

7. Romick, C. and Aslam, T., "High-Order Shock-Fitted Detonation Propagation in High Explosives," *Journal of Computational Physics*, Vol. 332, pp. 210–235, 2017.

8. Bdzil, J., Henninger, R. and Walter, J., "Guide for Input and output to the DSD Package," Technical Report LA-14278-MS, Los Alamos National Laboratory, Los Alamos, NM, USA, 2006.

9. Preston, D., Tonks, D. and Wallace, D., "Model of Plastic Deformation for Extreme Loading Conditions," *Journal of Applied Physics*, Vol. 93, pp. 211–220, 2003.

10. Berndt, M., Kucharik, M. and Shashkov, M., "Using the Feasible Set method for Rezoning in ALE," *Procedia Computer Science*, Vol. 1, pp. 1879–1886, 2010.

Fig. 3: Cylinder test geometry (from L to R): at 0, 10, 20, 30, 40, and 50 μs

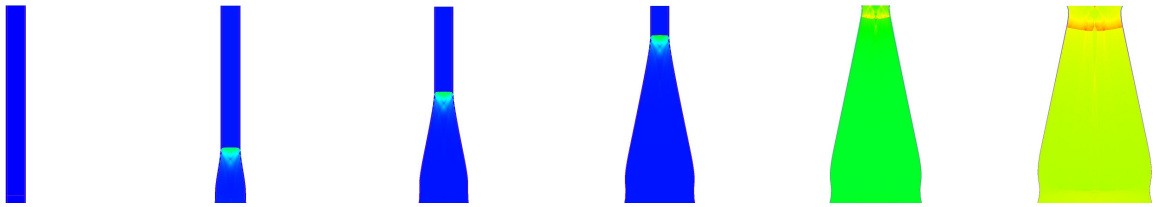

Fig. 4: Cylinder test pressure field (from L to R): at 0, 10, 20, 30, 40, and 50 μs

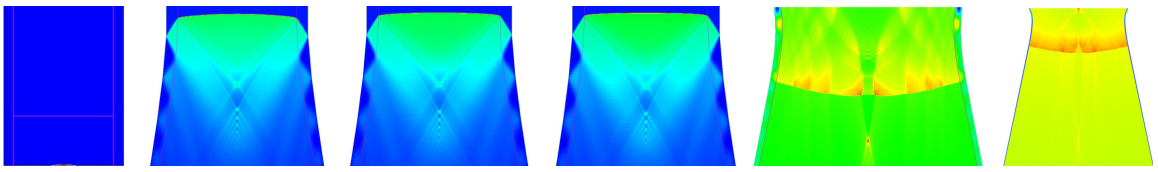

Fig. 5: Enlargements from Fig. 4 (from L to R): at 0, 10, 20, 30, 40, and 50 μs. These images are not all drawn at the same geometric scale.

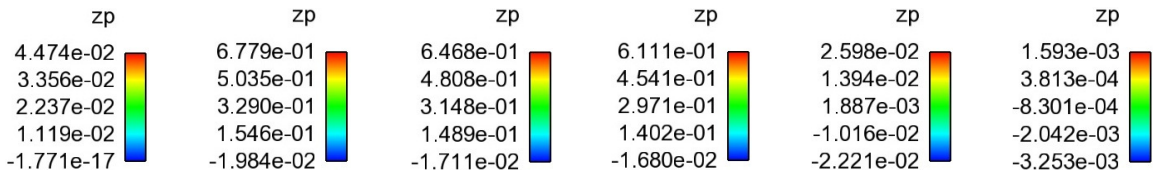

Fig. 6: Legend palette corresponding to Figs. 4, and 5 (from L to R): 0, 10, 20, 30, 40, and 50 μs. Pressure in Mbar.

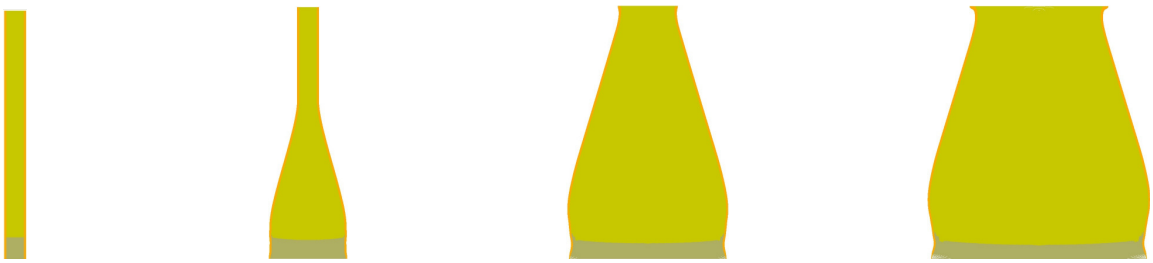

Fig. 7: Slab test geometry (from L to R): at 0, 10, 20, 27 μs

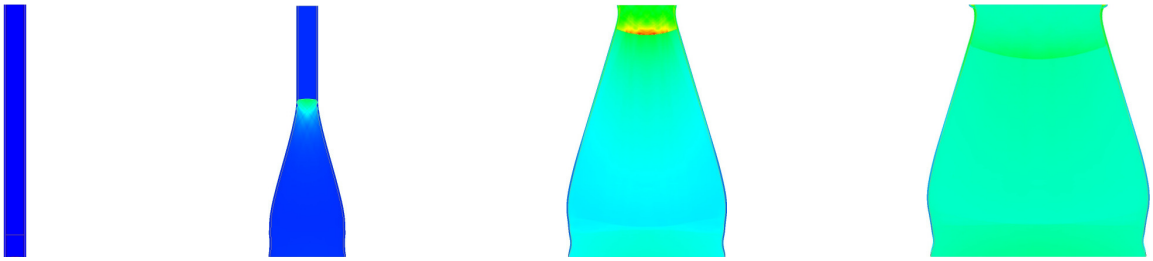

Fig. 8: Slab test pressure field (from L to R): at 0, 10, 20, 27 μs

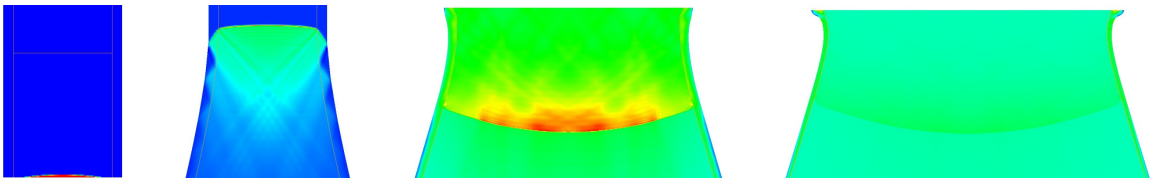

Fig. 9: Enlargements from Fig. 8 (from L to R): at 0, 10, 20, 27 μs. These images are not all drawn at the same geometric scale.

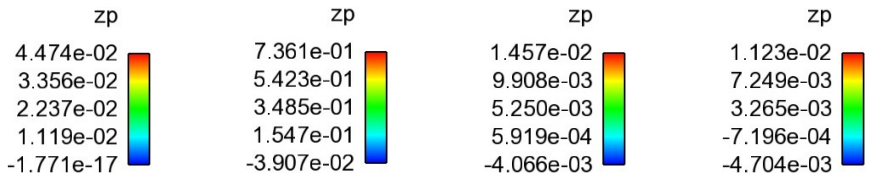

Fig. 10: Legend palette corresponding to Figs. 8, and 9 (from L to R): 0, 10, 20, 27 μs. Pressure in Mbar.

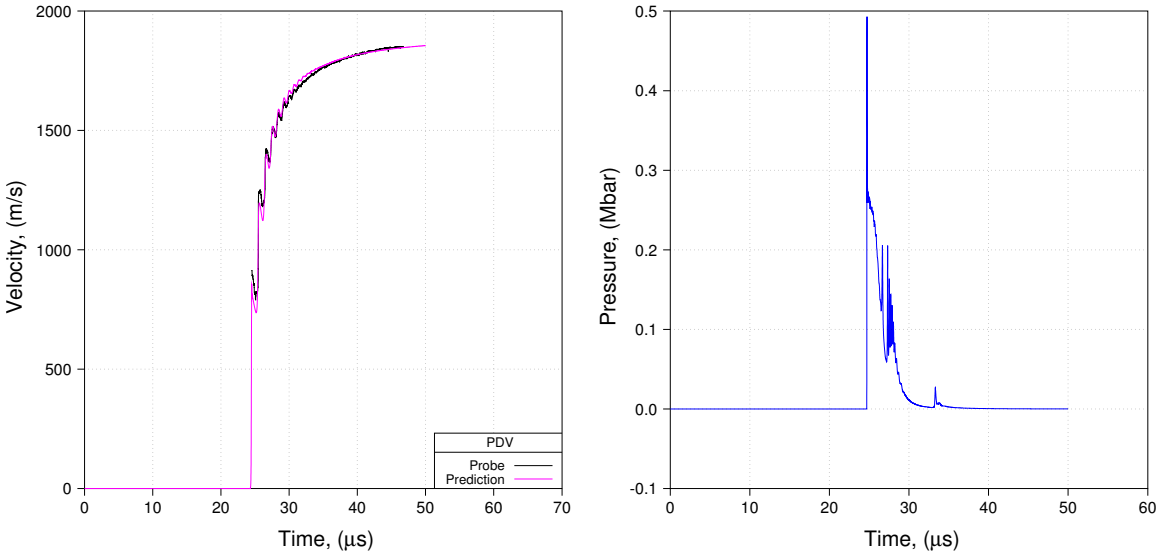

Fig. 11: Cylinder test simulation results: Left – free surface velocity compared to data from Probe 03; Right – pressure history at r,z point (0,21).

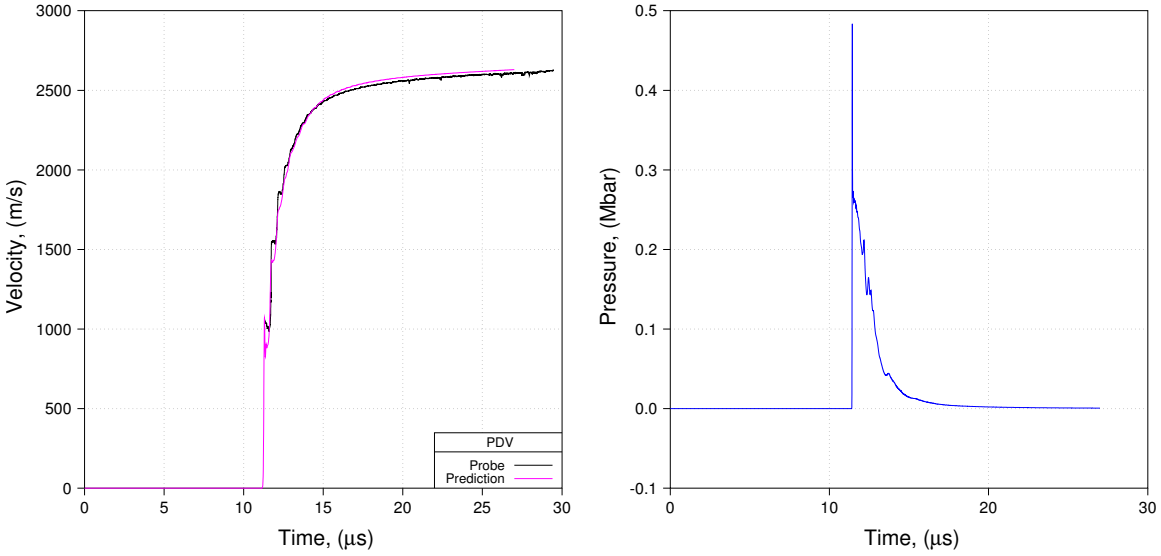

Fig. 12: Slab test simulation results: Left: free surface velocity compared to data from Probe 03; Right: pressure history at x,y point (0,9)

Question from Robert Dorgan, AFRL

Could this experiment be used for large critical diameter materials as a less expensive alternative to the CYLEX?

Answer from the authors

The slab test was intended to provide an alternative geometry for model validation where the detonation front curvature at breakout is along one principal axis rather than two, not to realize cost savings. However, there may be some cost savings in cases where the cost of the explosive is relatively low such that the Copper is a significant portion of the test cost.

As the test thickness is scaled up for the case of a large critical diameter explosive, it is important to select the other dimensions carefully to maintain 1D front curvature at breakout while also performing detonation velocity and confiner velocity measurements where the detonation is steady. Meeting both of these requirements becomes more difficult as the critical diameter increases. This is because thick slabs tend to require longer run distances to achieve steady detonation, but longer run distances allow more time for release waves from the edges of the experiment to influence the curvature at the center of breakout. For this reason, very thick slabs would require charge size increases both parallel and perpendicular to detonation propagation, possibly negating any cost savings.

We note also that the slab geometry involves a much shorter test time and exhibits less ringing in the wall. It is better able to access the higher pressure region of the product isentropes, but does not yield as much data for the middle-to-lower pressure region.